Study of the Self-assembly Process of an oligo(ethylene glycol)-thioacetyl Substituted Theophylline (THEO) on Gold Substrates.

Guadalupe Sánchez-Obrero[1], Miriam Chávez[1], Rafael Madueño[1], Manuel Blázquez[1], Teresa Pineda[1], Juan Manuel López-Romero[2], Francisco Sarabia[2], Jesús Hierrezuelo[2], and Rafael Contreras[2]*

[1] Department of Physical Chemistry and Applied Thermodynamics. Institute of Fine Chemistry and Nanochemistry. University of Cordoba, Campus Rabanales, Ed. Marie Curie 2ª Planta, E-14014 Córdoba, Spain

[2] Department of Organic Chemistry. Faculty of Sciences, University of Málaga, 29071 Málaga, Spain

Author e-mail address tpineda@uco.es

Author ORCID Nº: 0000-0002-1504-903X

Phone number: +34-957-218646

Fax number: +34-957-218618

KEYWORDS: self-assembled monolayer; polyoriented and single crystal gold electrode; cyclic voltammetry; electrochemical impedance spectroscopy; infrared absorption-reflection spectroscopy; X ray photoelectronic spectroscopy.

Abstract

A new oligo(ethylene glycol)-thioacetyl substituted theophylline (THEO) has been synthesized and used to form self-assembled monolayers (SAMs) on different gold substrates. The THEO-SAMs formed are compact and passivate the gold surface in an important extension. The thioacetyl group can be deprotected to release the mercapto-derivative that gives place to Au-S bond either in the absence or in the presence of base. Evidences that the THEO molecules bind to gold as thiolates are given by the behavior of the reductive desorption process of the SAM as a function of solution pH. However, some of the molecules can suffer breakage in the C-S position releasing thioacetic acid and the fragment oligo(ethylene glycol)-theophylline that can´t bind to gold. The thioacetic acid generated at the gold surface can be catalytically decomposed to acetyl and atomic sulfur. The later can be bound to gold as it has been demonstrated by electrochemical as well as by XPS techniques. The resulting THEO-SAM has been structurally characterized by IRRAS. Comparison of the IRRAS with the spectrum of the bulk molecules allows us to conclude about some degree of organization of the THEO chains upon SAM formation. The results of this study can be translated to a gold nanomaterial conjugate to be assayed in studies of theophylline derivatives drug delivery in living systems.

1. Introduction

Theophylline is a xanthine that acts as adenosine receptor antagonist and phosphodiesterase inhibitor and is used as bronchodilator in the treatment of asthma and chronic obstructive pulmonary disease [1]. Moreover, as other purine derivatives, it is also recommended as drug against Mycobacterium tuberculosis [2] as well as like anti-arthritic [3]. Low-dose theophylline exerts anti-inflammatory effects [4] although certain side-effects have been occasionally found as acute encephalopathy [5]. Thus, the concentration of theophylline must be strictly controlled under an acceptable therapeutic range. Many groups are involved in the construction of sensor systems to prevent the toxic side effects of over-dosed theophylline [6-9]. The narrow concentration range useful for this drug has encouraged the preparation of different drug-clay hybrid system (theophylline-smectite) to prove if it can be released under simulated gastric conditions. However,

an incomplete reversibility of the interaction process due to chemisorption of the drug within the clay system has been found that do not allow the correct delivery process [10].

One of the most popular strategies to improve the therapeutic effect of drugs is the covalent attachment of ethylene glycol oligomers to the therapeutic agents [11]. The technique of covalently attaching polyethylene glycol (EG) to a molecule is known as "PEGylation" and is now a well-established method in the field of targeted drug delivery systems [12]. To make EG attachments releasable, the conjugate must be chemically or enzymatically transformed into their active form after administration [11]. In these sense, multidrug PEG-conjugates [13] with dexamethasone and theophylline covalently linked to the same PEG unit has proved to show a slow degradation rate in simulated gastro-intestinal fluids and to permeate the intestinal membrane easier than the pure drugs [14, 15].

We have recently prepared oligo(ethylene glycol)-alkene substituted theophyllines and characterize them upon adsorption in the surface of porous and dense support membranes [16-18]. In the present work, we have used an EG spacer connected, in an extreme, to a theophylline moiety through the N7 position and a terminal thioacetyl group (THEO) (Scheme 1) to probe this molecule as a candidate to form self-assembled monolayers on gold substrates. The synthetic strategy to get the THEO molecule has been the use of an acetyl protecting group for the terminal thiol to avoid either disulfide bond formation or other unwanted side-reactions. Under these circumstances, the generation of free thiols to form well-packed SAMs would require the in situ deprotection of thioacetyl by acid or basic treatments [19-24]. The characterization of the THEO-SAM built in either a polyoriented or single crystals Au electrodes has been carried out by electrochemical techniques such as cyclic voltammetry, electrochemical impedance spectroscopy and differential capacity curves as well as infrared absorption-reflectance and X-ray photoelectron spectroscopies.

2. Experimental section

2.1. Chemicals.

Theophylline (Sigma-Aldrich, T1633) and tetraethylene glycol ditosylate (Sigma Aldrich, 341703) were used as starting materials. Semiconductor grade purity sodium hydroxide were purchased from Sigma-Aldrich. The rest of the reactants were from Merck analytical grade. All solutions were prepared with deionized water produced by Millipore system.

2.2. Synthesis of THEO.

Synthesis of THEO has been carried out in two steps, first, N7 activation and addition of the EG-tosyl derivative, and second protection of the oxygen terminal atom with the thiocetyl moiety (Scheme 1).

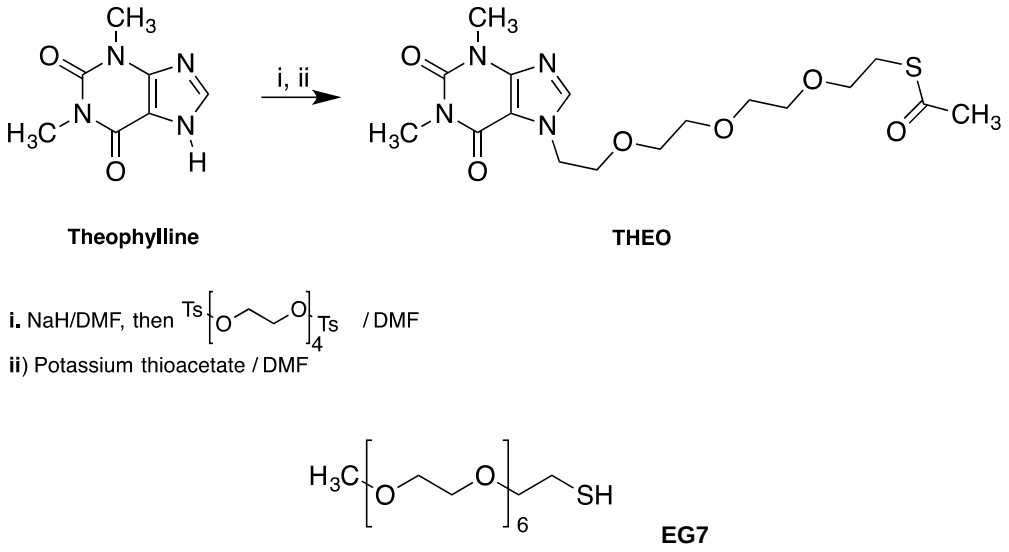

Scheme 1. Structure of the THEO and EG7 molecules

Under an argon atmosphere, NaH 60 % (0.49 g, 12.21 mmol) was added over a solution of theophylline (2 g, 11.10 mmol) in DMF (70 mL). After H_2 production ceased, a solution of tetraethylene glycol ditosylate (27.82 g, 55.5 mmol) in DMF (200 mL) was added. The mixture of reaction was stirred at 20 ºC during 12 h. After this period, crude was extracted with CH_2Cl_2 (3 x 50 mL) and washed with water (3 x 30 mL) and brine (2 x 50 mL). Organic phase was dried over anhydrous $MgSO_4$, filtered and concentrated to dryness under vacuum. The residue was purified by column chromatography (CH2Cl2/MeOH 98:2) to obtain 7-(2-(2-(2-(2-tosylethoxy)ethoxy) ethoxy)ethyl)theophylline (4.12 g, 73 %) as a colorless oil. NMR 1H ($CDCl_3$) δ (ppm): 7.78 (d, J = 8.0 Hz, 2H, Ar), 7.75 (s, 1H, H-8), 7.31 (d, J = 8.0 Hz, 2H, Ar), 4.02 (m, 16H, OCH_2), 3.53 (s, 3H, NCH_3), 3.38 (s, 3H, NCH_3), 2.42 (s, 3H, CH_3). NMR 13C ($CDCl_3$) δ (ppm): 155.7 ppm (C=O), 151.5 (C=O), 149.1 (C), 145.1, 142.9 (C8), 142.0 (C), 130.1, 128.3 (CH), 106.8 (C5), 71.0, 70.8, 70.7, 69.71, 69.69, 69.0 (CH_2), 47.1 (CH_2N), 30.1 (NCH_3), 28.2 (NCH_3), 21.9 (CH_3). IR (KBr) ν (cm^{-1}): 2869, 1701, 1656 cm^{-1}. UV (MeOH) λ_{max} (log ε): 274 nm (1.48), 208 (3.95).

Under an argon atmosphere, 7-(2-(2-(2-(2-tosylethoxy)ethoxy)ethoxy)ethyl)theophylline (606 mg, 1.19 mmol) in anhydrous DMF (30 mL) was treated at 20 ºC with potassium thioacetate (3.57

mmol, 407.5 mg). Then, the mixture of reaction was stirred for 12 h at 60 ºC. After this period, HCl 5 % (20 mL) was added and the mixture extracted CH_2Cl_2 (3 x 10 mL). Extracts were washed with water (3 x 10 mL), dried over anhydrous $MgSO_4$, filtered and concentrated to dryness under vacuum. THEO was isolated as a yellowish syrup (0.34 g, 68 %) by column chromatography (CH_2Cl_2/MeOH 98:2). NMR 1H ($CDCl_3$) δ (ppm): 7.70 (s, 1H, H-8), 3.58 (m, 16H, OCH_2), 3.57 (s, 3H, NCH_3), 3.38 (s, 3H, NCH_3), 2.31 (s, 3H, CH_3). NMR 13C ($CDCl_3$) δ (ppm): 195.3 (SC=O), 155.2 ppm (C=O), 151.6 (C=O), 148.7 (C4), 142.4 (C8), 106.4 (C5), 70.46, 70.41, 70.38, 70.18, 69.7, 69.31, 46.7 (CH_2N), 30.4 (CH_3), 29.7 (NCH_3), 28.7 (CH_2S), 27.8 (NCH_3). IR ν (cm^{-1}): 2921, 2851, 1691, 1353, 1127, 957 cm^{-1}. UV (CH_2Cl_2) λ_{max} (log ε): 274 nm (4.49), 230 (4.70). Exact mass for $C_{17}H_{26}N_4O_2S$ 414.1573; found 414.1578.

2.3. Methods.

Electrochemical experiments were performed using an Autolab (Ecochemie model Pgstat20) instrument attached to a PC with proper software (GPES and FRA) for the total control of the experiments and data acquisition. A conventional three electrodes cell comprising a platinum coil as the counter electrode, a saturated calomel electrode as the reference electrode and a gold (either polyoriented or single crystals (111), (100) and (110)) as the working electrode were used. The polyoriented gold electrode was a homemade sphere with a diameter of approximately 2 mm with a gold wire, grown by melting a high-purity Au wire (99.9998%). Gold single crystals were approximately 3-mm in diameter and 2 mm thick cylinders with a flat polished side oriented in the (111), (100) or (110) directions (Metal Crystals and Oxides Ltd). Before each electrochemical measurement, the electrode was annealed in a natural gas flame to a light-red melt for about 20 s and, after a short period of cooling in air, quenched in ultrapure water. The electrode was then transferred to the electrochemical cell with a droplet of water adhering to it to prevent contamination. The configuration of the sample consists of the contact of the single crystal gold faces with the solution by the hanging meniscus method. The surface condition was confirmed by a cyclic voltammogram in 0.01M $HClO_4$, and the real surface area was determined from the reduction peak of oxygen adsorption on the Au electrode. This surface treatment was the most appropriate for producing a surface that was clean, ordered, and very reproducible.

X-ray photoelectronic spectroscopy (XPS) analyses were performed with a SPECS Phoibos 150 MCD spectrometer (SCAI, University of Cordoba) using nonmonochromatized (12 kV, 300 W) Mg KR radiation (1253.6 eV). The THEO-SAM electrode was mounted on a steel sample holder

and introduced directly into the XPS analytical chamber. The working pressure was <5 × 10-9 Pa. The spectra were collected using a take-off angle of 45° with respect to the sample surface plane. The spectrometer was calibrated assuming the binding energy (BE) of the Au $4f_{7/2}$ line at 84.0 eV. The standard deviation for the BE values was 0.2 eV. Survey scans were run in the 0-1100 eV range (pass energy = 60 eV), while detailed scans were recorded for the S 2p, C 1s, C 1s and O 1s regions. The analysis involved linear background subtraction, and whenever necessary, spectral deconvolution was carried out by nonlinear least-squares curve fitting, adopting a Gaussian sum function.

HRMS were recorded with a Micromass (Autospec-Q) spectrometer. 1H and 13C NMR spectra were recorded with a 400 MHz ARX 400 Bruker spectrometer by using the residual solvent peak in CDCl3 (δ 7.24 ppm, 400 MHz, for 1H and δ = 77.0 ppm, 100 MHz, for 13C). TLC analyses were performed on Merck silica gel 60 F 254 plates, and column chromatography was performed on silicagel 60 (0.040–0.063 mm).

IRRAS Characterization. A 250 nm thick Au layer adhered to a 2.5 nm thin chromium layer deposited on a Borosilicate glass 11x11 mm flat surface were used as Au(111) coated substrates (Gold Arrandee^{TM}) for the Infrared Reflection-Absorption Spectroscopy (IRRAS) measurements. IRRA spectra were recorded on a JASCO 6300 FTIR single (He-Ne) laser beam spectrometer in the 400-4000 cm-1 wavenumbers range at a resolution of 4 cm-1, and the data were acquired by the integrated software (Spectra Manager). A variable angle specular reflectance accessory (Pike Technologies-VeeMAXTM) assembled in the FTIR spectrometer compartment enabled samples to be analyzed at different beam incident angles. The dried Au substrates were placed face downwards on a mask platform with an aperture (10 mm in diameter) to define the position and sampling dimensions where the beam spot was collimated. A p-polarized laser beam at a grazing angle of 80° was used to interact with the sample surface for enhancement of the IR signals collected by the MCT-detector. Prior to the measurements, the interferometer and the sample compartments were purged with a dry and free CO_2 air flux of 8 l/min supplied by a compressed air adsorption dryer (K-MT LAB, Parker/Zandet GmbH&Co.KG).

2.4. THEO-SAM formation.

The SAMs were formed by contacting the gold substrates, either by the immersion (polyoriented substrates) or the meniscus method (single crystals), with an ethanolic 2.5 mM THEO solution for the desired modification time.

3. Results and discussion

3.1. General characterization of the THEO-SAM.

The formation of SAMs from acetyl-thioesters requires the generation of the thiolates to get the S-Au bond. This thiol group deprotection reaction can be favored in the presence of a base [24]. In this work, we have assayed the formation of the SAM by using three methods: a) from an ethanol solution without using base, b) from a THF solution containing Et_4NOH and, c) from a THF solution containing Et_3N. To obtain the SAMs, the Au electrodes were immersed in the above solutions that also contained THEO 2.5 mM for 24 h. After that, the modified electrodes were transferred to the electrochemical cell and equilibrated at 0.05 V with a 0.1 M phosphate buffer solution at pH 7 and then, cyclic voltammograms were recorded by scanning the potential to negative values. The obtained signals (Figure 1) should correspond to the reductive desorption process of the SAMs. As it can be observed, the three curves obtained for the SAMs built under different experimental conditions are almost identical with a peak potential at -0.82 V ± 0.01 V and a charge density of 78 ± 4 μC/cm^2. This charge density is very close to that obtained for the alkanethiol SAMs and is typical of densely packed monolayers formed by molecules in a stand-up configuration with a surface area of around 20 Å^2. This analysis is made by assuming that the reductive desorption process corresponds to the breaking of the Au-S bond as described by eqn. (1):

$$R\text{-}S\text{-}Au + 1e + 1H^+ \rightarrow R\text{-}SH + Au \qquad (1)$$

Under these circumstances, it can be said that the acetyl-thioesters are converted to the thiolates in the presence as well as in the absence of base and are able to chemisorb on the gold surface in a similar way. However, the theoretical fingerprint of the THEO molecule is bigger than that of the alkanethiol molecules. Thus, this measured charge density must contain some contributions that needs to be further analyzed (see below).

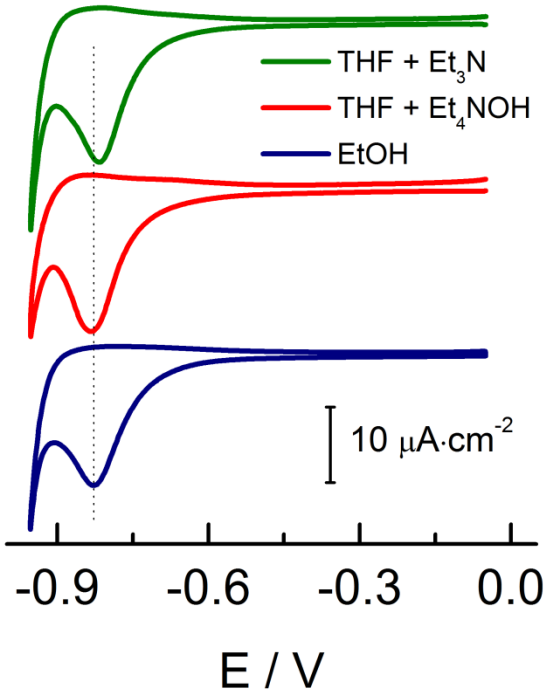

Figure 1. Cyclic voltammograms of the reductive desorption process of the THEO-SAMs formed from different solutions recorded in phosphate buffer solution at pH 7. Scan rate: 0.02 V/s.

To further check if the adsorbed species are the thiolates, a study of the reductive desorption process of the SAM formed in the absence of base, as a function of pH, has been carried out. The SAMs are formed from an ethanolic solution (at a modification time of 24 h), and after that, they are transferred to the electrochemical cell containing a buffer phosphate solution at different given pH. The voltammetric curves of the reductive desorption processes are showed in Figure 2. These signals are typical of this type of processes and show an increase in potential as the pH of solutions decreases. At pH < 4, the signal is hidden under the hydrogen evolution. The peak potentials plotted in Figure 2, follow a linear trend in the pH range from 4 to 10 with a slope of 56 mV / pH. This variation with pH suggests that an H^+ ion is involved in the reductive desorption process (eqn. (1)) and points to the fact that the species that desorbs is the thiolate that is rapidly protonated to yield the thiol, the stable species in solution under these conditions. At pH > 10 the thiolate becomes the stable species in solution and, thus, the peak potential is kept constant. This behavior can be taken as an additional evidence of the spontaneous breaking of the acetyl-thioester bond upon SAM formation.

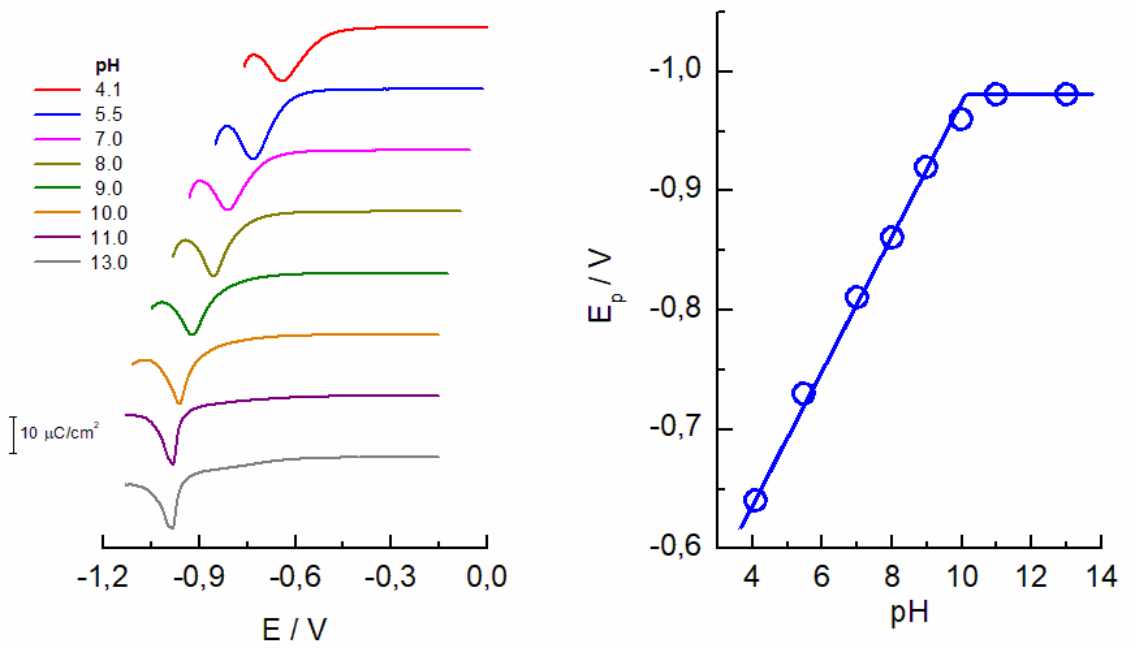

Figure 2. Cyclic voltammograms (left) and peak potentials (right) for the reductive desorption process of the THEO-SAMs as a function of solution pH. The THEO-SAMs are formed from ethanolic solution for a modification time of 24 h.

The sensitivity of the THEO-SAM to the substrate structure has been addressed by using single crystal gold surfaces. The process of reductive desorption has been demonstrated to be very dependent on the crystal facet of the Au substrate, the trend observed being consistent with the potential of zero charge at Au single crystal surfaces [25, 26].

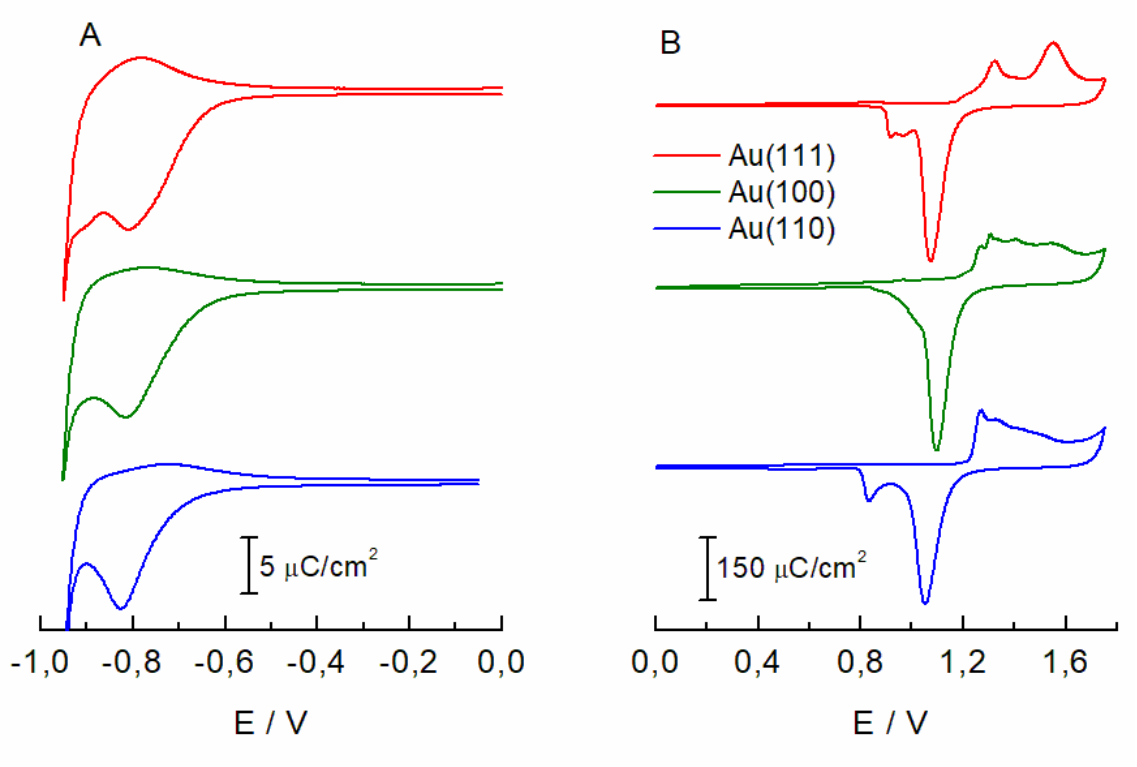

Figure 3. (A) Cyclic voltammograms for the reductive desorption process of the THEO-SAM formed from a ethanolic solution in Au single crystal electrodes of low index. (B) Voltammetric profiles of the same Au single crystal electrodes used recorded in 10 mM perchloric acid solution.

Figure 3 shows the cyclic voltammograms for the reductive desorption process for the THEO-SAMs formed in Au(111), Au(100) and Au(110) single crystal electrodes. The electrochemical profile of the Au single crystals in $HClO_4$ 10 mM are also plotted to account for the different surface structures. Contrary to our expectations, there is very little influence of the surface structure on the shape of the curves. The peak potentials are also very similar, that is, -0.810, -0.816 and -0.826 V for the SAMs desorbed from Au(111), Au(100) and Au(110), respectively. Moreover, the half-width of the curves is higher than 100 mV as it also occurs in the polyfaceted surface (see Figure 1). The broad desorption peaks indicate that the SAMs are disordered as it would be expected from the structure of the THEO molecules (Scheme 1). In fact, the THEO molecule possesses a tri-ethylene glycol arm that, in the absence of the theophylline attached in the terminal region, presents a helicoidal conformation. However, with this terminal group attached by its N7 position, the organization of the EG arm can be different as this bulky terminal group should add and additional disorder to the SAM. To ascertain if this behavior originates on the disorganization

of the molecular arm or because of the presence of the terminal group, a SAM formed from EG7 (Scheme 1) has been examined. The EG7-SAM has been prepared from an ethanolic solution and the reductive desorption has been carried out in alkaline media. The cyclic voltammogram has been recorded and plotted in Figure 4 together with this obtained for the THEO-SAM under the same experimental conditions. As it can be seen, the observed profile for the EG7-SAM shows a fine structure that contrasts with the broad peak observed for the Theo-SAM. Thus, a strong influence of the bulky terminal group is concluded for the different behavior of these two desorption profiles.

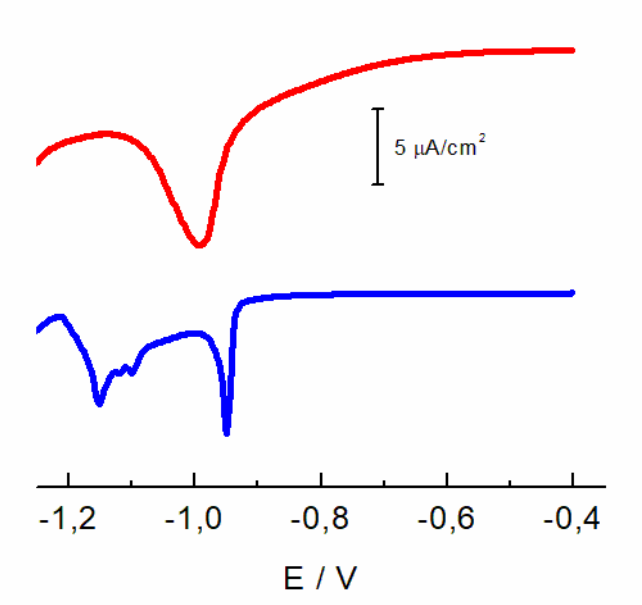

Figure 4. Cyclic voltammograms for the reductive desorption process of (red) THEO- and (blue) EG7-SAMs in KOH 0.1 M media.

In addition, there is another result that deserves attention. The charge densities involved in the reductive desorption processes of these two molecules are very different (Q(THEO) = 78 µC/cm^2 and Q(EG7) = 48 µC/cm^2). These charge densities allow us to determine the molecular area of these molecules as 20.5 and 33.4 Å^2 for THEO and EG7, respectively. Even if the fingerprint of both molecules were assumed to be the same, the different molecular area obtained from the reductive desorption method has nonsense. In fact, the reverse result would be obtained based on the presence of the theophylline group in the terminal THEO molecule. Thus, an effect not considered up to now is necessary to be analyzed. As it has been explained above, the generation

of the thiolate to form the Au-S bond, requires the releasing of the acetyl group. However, another possibility is that the subsequent S-C bond be broken and thioacetic acid can be released. If this were the case, the thioacetic acid molecule can also react with the gold surface and, as it has been well documented, the cleavage of the S-C bonds can be catalyzed by Au [27]. Vela et al. [28] have studied the adsorption of thioacetic acid on Au(111) from organic solutions to find the effect of the functional group on the stability of the S-C and S-Au bonds. They found that the molecule is first physisorbed to the Au(111) surface as an intermediate that evolves to form a free non-thiolated molecule and the chemisorbed monomeric S atom. Thus, it can be proposed that the extra charge density obtained in the reductive desorption process of the THEO-SAM should be due to the presence of some adsorbed S atoms in the form of an ad-layer together with the THEO-SAM. If the extra charge density obtained for the THEO-SAM desorption in respect to the theoretically expected for a full monolayer of molecules with a fingerprint of around 29 $Å^2$ is taken into account, 83 % of the charge density should correspond to THEO molecules desorption and the extra 17 % to S atoms. It can be assumed that some of the THEO molecules are adsorbed through the S-Au bond and, an important portion (up to 17 %) are as S atoms that can be desorbed through the following reaction [29, 30]:

$$S\text{-}Au + 2e \rightarrow S^{=} + Au \qquad (2)$$

To check if this hypothesis is true and elucidate the nature of the adsorbates, a study of XPS of the THEO-SAM has been carried out. Figure 5 shows the spectra of the S 2p core-level peak of the THEO-SAM taken under different experimental conditions. Attempts to fit the experimental data to one doublet corresponding to S-Au bond at 161.8/163.0 eV was unfruitful. The best fitting of the peak shows that at least three doublets centered at 161.0, 162.0 and 163.8 eV are needed. These peaks are assigned to that corresponding to atomic monomeric sulfur bound to gold, gold-sulfur and free thiol or sulfide [31-33], respectively. No oxidized sulfur species have been found at higher binding energies [34].

The atomic sulfur can be produced either by C-S bond cleavage once the mercaptoderivative is adsorbed to the gold surface after the acetyl group has been released [35, 36], or by the breakage of the S-C bond that deliver thioacetic acid that is prone to suffer a cleavage on the gold surface, leaving the S atom attached to it [28]. The reduction of the S species can be observed as broad peaks located at -0.95 to -1.15 V [29]. In the present case, the existence of adsorbed sulfur is hard to see as the reduction coincides with that of the THEO molecules. Then, we have checked if the

treatments commented above to obtain a clean cleavage of the acetyl protecting group can be evaluated by XPS. We have prepared a layer using the method (b) of preparation (THF solution containing Et_4NOH) and the obtained spectrum is shown in Figure 5B for the S 2p signal. Although the fitting of this peak requires the inclusion of the three already mentioned contributions, it is interesting to highlight that the ratio of S-Au bond is now much more important in the spectrum. In fact, the peak due to adsorbed sulfur goes from 20 % in the THEO-SAM formed from ethanol solution to 6 % in THF-Et_4NOH. Moreover, the amount of free thiol or sulfide is also decreased from 30 to 21 % under these conditions. Then, it can be concluded that the XPS technique is more precise to check the SAM quality than the electrochemical reductive desorption methodology when using acetyl-protected molecules.

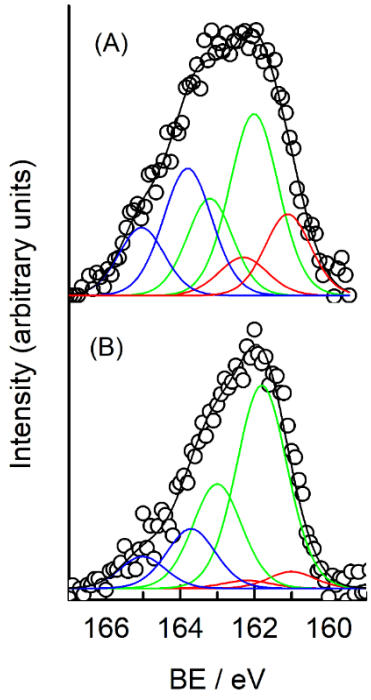

Figure 5. XPS spectra for the S 2p region of a THEO-SAM formed on an Au substrate in an ethanolic (A) and THF+Et_4NOH (B) solutions. Raw data (o); fitted spectra, black line; Doublets for Sulfur (red), S-Au bond (green) and free thiol or sulfide species (blue).

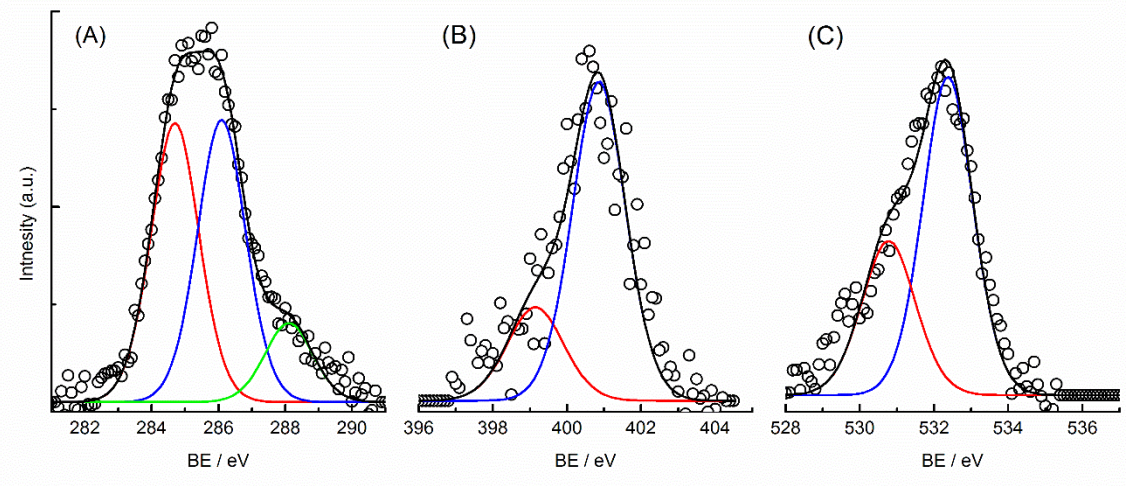

Figure 6. C 1s (A), N 1s (B) and O 1s (C) XPS spectra of the THEO-SAM formed in THF+Et_4NOH (o). The spectra are decomposed into individual contributions (colored lines) and the black solid lines are the overall fit.

The analysis of the peaks due to C 1s, O 1s and N 1s (Figure 6) can also help to establish the nature of the SAM. The C 1s peak shows an asymmetric shape centered at 285 eV with a shoulder in the high BE region. Three components have been used to fit the data. Zharnikov et al. [37] have studied the XPS of a series of acetyl-protected dithiols derivatives and the effects of the different deprotection methodologies. They found a peak at 287.6 eV that they assigned to the acetyl protection groups which were not removed and that should be located at the SAM ambient interface. The presence of a peak at 288.1 eV in the C 1s spectrum should means that some pristine THEO molecules are present in the preparations. This fact agrees with the S 2p peak at 163.8 eV that can be assigned to the sulfide groups. Two major peaks at 284.7 and 286.1 eV can be assigned to alkyl (C-C) and etheric (C-O) carbon atoms, respectively [38]. The last component should correspond to the EG part of the monolayer [39, 40] whereas the first one can be attributed to carbon contamination [41]. The N 1s signal has been deconvoluted into two components at 399.2 and 400.8 eV that should correspond to pyridinic (-N=) and pyrrolic nitrogen, respectively [42]. The ratio of the two peaks are 1:3, coinciding with the nitrogen types included in the THEO molecule. Finally, the signal of the O 1s peak can be deconvoluted into two peaks at 530.8 and 532.4 eV. These peaks can be attributed to carbonyl (C=O) and etheric (C-O) groups, respectively [39].

3.2. Blocking properties of the THEO-SAM

The presence of holes and defects in the monolayer has been checked by studying the behavior of the redox probe ferricyanide in the presence of the SAM. Figure 7 shows the cyclic voltammograms of ferricyanide in a bare and a modified poly-oriented gold electrode. The presence of the monolayer inhibits the electrochemical signal in a great extension and this inhibition is more important upon increasing modification time. The shape of the voltammetric curves indicates a decrease of the reversibility in the presence of the monolayer and, probably, absence of holes or defects as no signal is obtained at the potential around the formal potential of the redox probe.

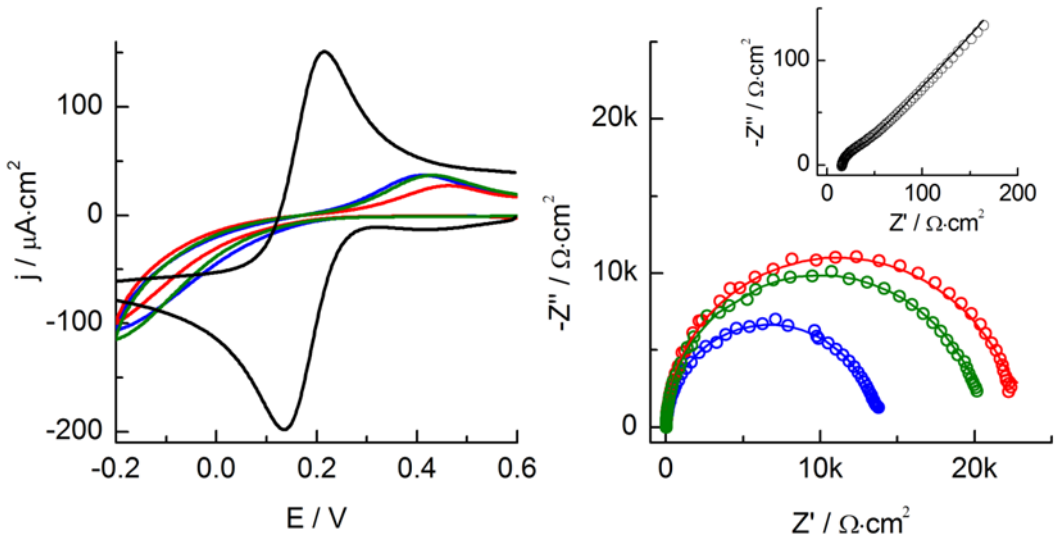

Figure 7. Cyclic voltammograms (left) and electrochemical impedance spectra (right) of ferricyanide in bare (black) and THEO-SAM modified gold electrode for 1 (blue), 3 (green) and (red) 15 h.

This evolution is more evident in the impedance spectra taken under the same experimental conditions. These spectra can be fitted by using a Randles circuit that consists of a double layer capacity (C_{dl}) in parallel to a charge transfer resistance (R_{ct}) and Warburg impedance (Z_W) (Scheme 2). This parallel combination of R_{ct} and C_{dl} gives a Nyquist plot consisting of a semicircle at high frequencies and a linear region at lower frequencies indicating mass transport behavior. In this way, the Nyquist plots corresponding to the monolayer-modified electrode would show an increase of the semicircle in parallel with the inhibition of the electron-transfer process. Moreover, the absence of the linear region at low frequencies agrees with the lack of defects mentioned above

and a complete blocking behavior by the monolayer. As it can be seen in Figure 7, the spectra obtained in the presence of the Theo-SAM only show semicircles covering the complete frequency range.

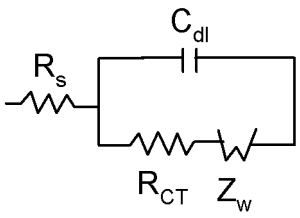

Scheme 2

The apparent rate constants of ferricyanide probe at different modification times are determined by using eqn. (3) [43], with the parameters having its usual meaning and the values obtained are gathered in Table 1.

$$R_{CT} = \frac{R \cdot T}{n^2 \cdot F^2 \cdot A \cdot k_{app} \cdot c} \qquad (3)$$

Comparing to the rate constant of ferricyanide measured with a naked electrode (~0.02 cm/s),[44] there are several magnitude order of decrease in the presence of the monolayer. However, the occurrence of tunneling mechanism can be neglected as a high current is observed in the cyclic voltammograms. Moreover, the present layer contains molecules that have two portions of different chemical nature. On one hand, the theophylline moieties should be very conductive as it was observed for SAMs of mercaptopurine [45]. On the other hand, the EG chain has different properties. A recent study has reported a study of the charge tunneling across different SAMs of oligo(ethylene glycol)s and has stablished that the presence of multiple oxygen atoms in the backbone substantially decreases β, the tunneling coefficient, in relation to SAMs of matched length of n-alkanethiolates [46]. Thus, the observed decrease in the rate constant for electron transfer can be attributed to the presence of the EG3 arm and also to the good organization of the molecules in the SAM.

Table 1. Apparent ET rate constant of Ferricyanide in the presence of the THEO-SAM prepared a different modification time, as determined from the impedance data.

	t_{mod}		
THEO-SAM	1 h	3 h	15 h
k_{app} / $cm \cdot s^{-1}$	$2.03 \cdot 10^{-5}$	$1.32 \cdot 10^{-5}$	$1.22 \cdot 10^{-5}$

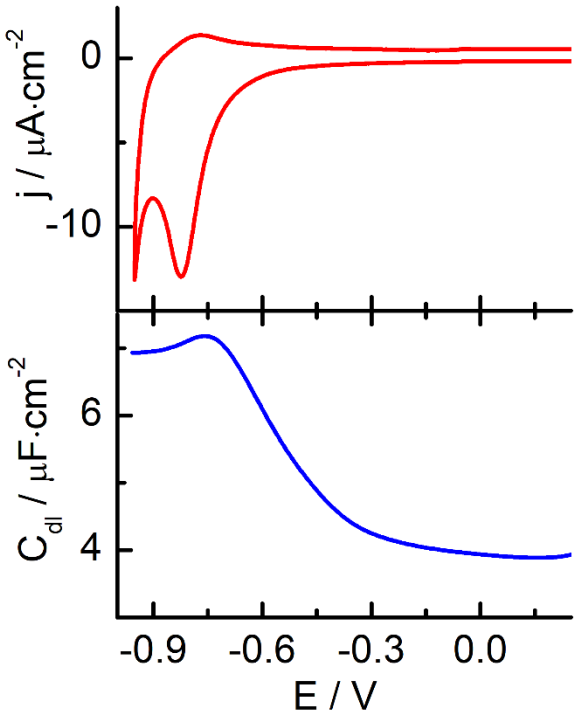

Figure 8. Changes in the double layer capacity (blue) for the THEO-SAM with potential, recorded in phosphate buffer solution at pH 7. The reductive desorption peak (red) of the THEO-SAM formed under the same experimental conditions is shown for comparison.

The monolayer double-layer capacitance curve has been measured to further evaluate the Theo-SAM compactness and thickness. The capacitance curve has been recorded starting at 0.25 V and scanning to negative values in the potential region where the reductive desorption process takes place. Figure 8 shows the double-layer capacitance (C_{dl}) curve obtained for a THEO-SAM formed

at a modification time of 15h from a ethanolic solution. The cyclic voltammogram for the reductive desorption process of the Theo-SAM obtained under the same experimental conditions as the C_{dl} curve is also shown in Figure 8 to localize the different events. A region with a lower and almost constant capacitance value (C_{dl} = 3.9 μF/cm^2) is observed that coincides with the double layer region in the cyclic voltammogram. This behavior is an indication of the existence of a compact layer that functions as a dielectric. However, this SAM is composed of two segments with very different properties. These kind of SAMs have been analyzed by using a model consisting of two capacitors in series with a total specific capacitance CSAM defined by [47]:

$$C_{SAM} = (C_{THEO}^{-1} + C_{EG}^{-1})^{-1} \quad (4)$$

where

$$C_{THEO} = \frac{\varepsilon_o \cdot \varepsilon_{THEO}}{d_{THEO}} \qquad C_{EG} = \frac{\varepsilon_o \cdot \varepsilon_{EG}}{d_{EG}}$$

In these eqn., C_{THEO} and C_{EG} are the specific capacitances of the corresponding THEO and EG segments, ε_o is the vacuum permittivity and ε and d, are dielectric constant and thickness of the corresponding segment, respectively.

We use ε_{THEO} and d_{THEO} as 11 and 8 Å [45, 48], respectively, taking advantage of the similarity between the theophylline and mercaptopurine moieties. With these values, we obtain a capacitance value of 12 μF/cm^2 for THEO. For the EG segment, the ε_{EG} and d_{EG} values of 4.8 and 9 Å are used [47]. Under these conditions, a value for C_{SAM} of 3.5 μF/cm^2 is calculated by using eqn. (4) that is close to the experimental value. Thus, it can be concluded that a compact Theo-SAM can be formed on the gold surface.

3.3. FT-IRRAS results.

The IR spectra of the THEO molecule in the low frequency region either in the KBr solid sample or attached to the gold surface are shown in Figure 9. The spectra contain many signals corresponding to the theophylline and the EG arm as well as the thio-acetyl groups.

The shoulder observed at 1725 cm^{-1}, that is absent in the THEO-SAM spectrum can be assigned to the C=O stretching mode of the thio-acetyl group in the starting compound. This assignation has been previously made by experimental and theoretical means [19, 49, 50]. The absence of this signal in the spectrum of the SAM is consistent with the breaking of the acetyl group previous to the adsorption of the THEO molecule.

The IR bands of the theophylline molecule have been assigned very recently [51]. The doublet observed at 1700/1685 cm^{-1} can be assigned to the C=O asymmetric stretching vibrations either

free or hydrogen bonded with N-H groups, respectively. In the SAM, only the peak corresponding to the free C=O group is observed that can be explained by the inaccessibility of the C=O and N-H groups upon SAM formation. The peak at 1657 cm^{-1} due to C=C ring stretching is conserved in the spectrum of the SAM. Other signals, such as 1547, 1425, 1272, 1193, 1061 cm^{-1}, assigned to ring vibrations modes are also observed in the spectrum of the THEO-SAM. Finally, the $-CH_3$ mode at 974 cm^{-1} disappears upon molecule immobilization. This fact can be explained by the orientation of these groups with respect to the gold surface.

The peaks observed for the molecular region corresponding to the EG arm can be assigned by using the literature data for poly-ethylene-glycol (PEG) [47, 52, 53]. In the spectrum of the THEO some bands at 1480 and 1460 cm^{-1} appear that have been assigned to EG CH2 scissor mode in the crystalline and amorphous PEG, respectively. These bands are also observed in the FT-IRRAS although they are weaker than in the KBr solid sample. The band at 1350 cm^{-1} (EG CH2 gauche) is also obtained in the monolayer but, in this case, a band at 1325 cm^{-1} also appears that is assigned to the C-C trans conformation of isolated groups [53]. This is an indication of the higher organization of the EG arm upon monolayer formation. At 1296 and 1249 cm^{-1}, the twist modes are observed as a shoulder of a more complex band and a sharp band, respectively, that are conserved in the monolayer. Finally, the region of 1050 to 1150 cm^{-1} contains the vibrations of C-O and C-C stretch modes. In the KBr solid sample spectrum, a broad band showing peaks at 1140, 1113 and 1096 cm^{-1} is obtained that gets sharper in the monolayer spectrum, that shows a main peak at 1134 cm^{-1} [47, 53-55].

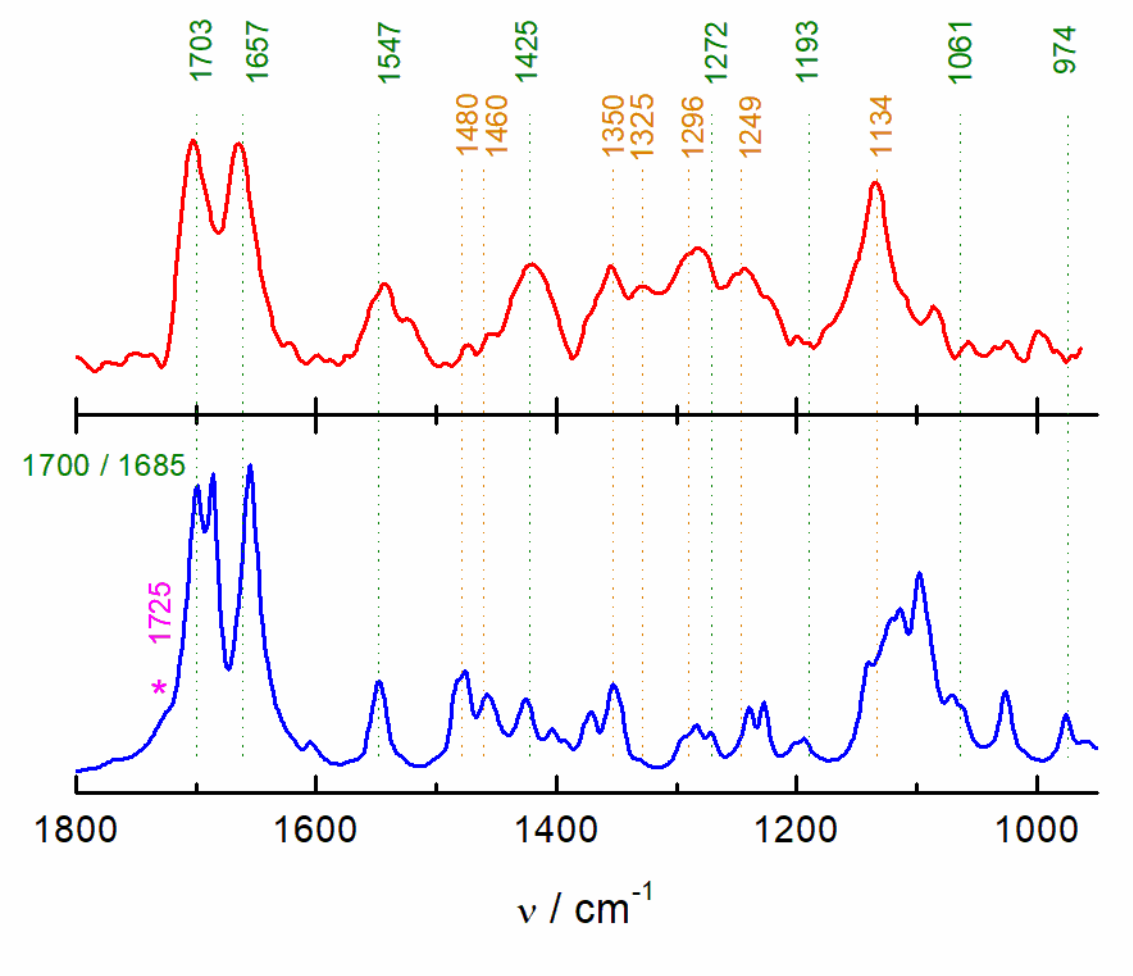

Figure 9. Infrared spectra of THEO in KBr solid (blue) and self-assembled in a Au(111) substrate (red). Labels correspond to: green: theophylline molecule; moiety groups; orange: EG arm; magenta: correspond to: EG arm groups; magenta: carbonyl of the thioacetyl group.

Thus, IRRAS spectrum of the THEO-SAM indicates that the THEO molecules are grafted to the gold surface but, it is not possible to get a deeper insight into the organization of the EG groups in the SAM as the peaks are broader and seem to contain contribution of different structures.

4. Conclusions

We have successfully prepared a self-assembled monolayer of a novel molecule, that bears a bulky terminal group (theophylline) that has been chosen because it possesses biological and pharmacological properties [14, 15, 18, 56, 57]. This active molecule is attached to an EG arm that can be bound to gold surfaces by means of the S-Au bond. The use of conjugation through EG

(PEGylation) is one of the most interesting methods to obtaining adducts that can be delivered in a more appropriate way either decreasing the uptake by the reticulo-endotelial system, prolonging blood residence, decreasing degradation by metabolic enzymes and reducing protein immunogenicity [58-60].

THEO-SAMs formed under different experimental conditions result in ordered architectures that passivate the metal surface mainly due to the molecular layer compactness. Electrochemical techniques such as cyclic voltammetry of the reductive desorption process indicate that THEO bind to the gold surface as thiolate species. The breakage of the C-S bond that liberates the mercapto-derivative takes place in the presence of base in the modification solutions as well as in the absence of that reactant. However, the final characteristics of the SAM are somewhat dependent on the composition of the modification solution. The combination of the different electrochemical methodologies together with XPS and IRRAS spectroscopies helped us to obtain the structural properties of the THEO-SAM.

It is interesting to note that the THEO-SAMs are not sensitive to the structural properties of the gold substrates either polyoriented or single crystals with different orientations. This means that layers with similar characteristics can be formed on gold nanomaterials of different size and shapes. These THEO conjugate nanomaterials can be used in assays of drug delivery in the site of action taken advantage of the low dose necessary for theophylline for the different treatments.

Acknowledgements. We thank the Ministerio de Economía y Competitividad (MINECO) (Projects CTQ2014-60227-R, CTQ2016-76311-R and CTQ-2015-71955-REDT Network of Excellence Sensors and Biosensors), Junta de Andalucía (P10-FQM-6408) and University of Córdoba for financial support of this work.

5. References

[1] D.J.F. Rowe, I.D. Watson, J. Williams, D.J. Berry, The Clinical Use and Measurement of Theophylline, Ann. Clin. Biochem., 25 (1988) 4-26.

[2] S.N. Mangasuli, K.M. Hosamani, H.C. Devarajegowda, M.M. Kurjogi, S.D. Joshi, Synthesis of coumarin-theophylline hybrids as a new class of anti-tubercular and anti-microbial agents, Eur. J. Med. Chem., 146 (2018) 747-756.

[3] A.G.A. Gaafar, B.A.S. Messiha, A.M.L. Abdelkafy, Nicorandil and theophylline can protect experimental rats against complete Freund's adjuvant-induced rheumatoid arthritis

through modulation of JAK/STAT/RANKL signaling pathway, Eur. J. Pharmacol., 822 (2018) 177-185.
[4] B.G. Cosio, A. Iglesias, A. Rios, A. Noguera, E. Sala, K. Ito, P.J. Barnes, A. Agusti, Low-dose theophylline enhances the anti-inflammatory effects of steroids during exacerbations of COPD, Thorax, 64 (2009) 424-429.
[5] M. Ogawa, K. Takano, K. Kawabe, M. Moriyama, H. Ihara, Y. Nakamura, Theophylline Potentiates Lipopolysaccharide-Induced NO Production in Cultured Astrocytes, Neurochem. Res, 39 (2014) 107-116.
[6] H. Jiang, K. Ling, X. Tao, Q. Zhang, Theophylline detection in serum using a self-assembling RNA aptamer-based gold nanoparticle sensor, Biosens. Bioelectron., 70 (2015) 299-303.
[7] Y.J. Yang, L. Guo, W. Zhang, The electropolymerization of CTAB on glassy carbon electrode for simultaneous determination of dopamine, uric acid, tryptophan and theophylline, J. Electroanal. Chem., 768 (2016) 102-109.
[8] S. Feng, C. Chen, W. Wang, L. Que, An aptamer nanopore-enabled microsensor for detection of theophylline, Biosens. Bioelectron., 105 (2018) 36-41.
[9] J. Wang, W. Cheng, F. Meng, M. Yang, Y. Pan, P. Miao, Hand-in-hand RNA nanowire-based aptasensor for the detection of theophylline, Biosens. Bioelectron., 101 (2018) 153-158.
[10] V. Trivedi, U. Nandi, M. Maniruzzaman, N.J. Coleman, Intercalated theophylline-smectite hybrid for pH-mediated delivery, Drug Deliv. Transl. Re., (2018).
[11] W. Li, P. Zhan, E. De Clercq, H. Lou, X. Liu, Current drug research on PEGylation with small molecular agents, Prog. Polym. Sci., 38 (2013) 421-444.
[12] P. Mishra, B. Nayak, R.K. Dey, PEGylation in anti-cancer therapy: An overview, Asian J. Pharma. Sci., 11 (2016) 337-348.
[13] M. Zacchigna, G. Di Luca, F. Cateni, V. Maurich, M. Ballico, G.M. Bonora, S. Drioli, New MultiPEG-conjugated theophylline derivatives: Synthesis and pharmacological evaluations, Eur. J. Pharm. Sci., 30 (2007) 343-350.
[14] M. Zacchigna, F. Cateni, D. Voinivich, M. Grassi, S. Drioli, G.M. Bonora, New multidrug (dexamethasone and theophylline) PEG-conjugate: synthesis, in vitro release studies and intestinal permeability, J. Drug Del. Sci. Tech., 19 (2009) 177-184.

[15] M. Grassi, G.M. Bonora, S. Drioli, F. Cateni, M. Zacchigna, Pharmacokinetic analysis of multi PEG-theophylline conjugates, Comput. Biol. Chem., 40 (2012) 7-14.
[16] J. Hierrezuelo, V. Romero, J. Benavente, R. Rico, J.M. López-Romero, Membrane surface functionalization via theophylline derivative coating and streptavidin immobilization, Colloids Surf., B, 113 (2014) 176-181.
[17] M.I. Vázquez, V. Romero, J. Benavente, R. Romero, J. Hierrezuelo, J.M. López-Romero, R. Contreras-Cáceres, Characterization and stability of a bioactivated alumina nanomembrane for application in flow devices, Microporous Mesoporous Mater., 226 (2016) 88-93.
[18] J. Hierrezuelo, J.M. Lopez-Romero, R. Rico, J. Brea, M.I. Loza, C.Z. Cai, M. Algarra, Synthesis of theophylline derivatives and study of their activity as antagonists at adenosine receptors, Bioorg. Med. Chem., 18 (2010) 2081-2088.
[19] J.M. Tour, L. Jones, D.L. Pearson, J.J.S. Lamba, T.P. Burgin, G.M. Whitesides, D.L. Allara, A.N. Parikh, S. Atre, Self-Assembled Monolayers and Multilayers of Conjugated Thiols, .alpha.,.omega.-Dithiols, and Thioacetyl-Containing Adsorbates. Understanding Attachments between Potential Molecular Wires and Gold Surfaces, J. Am. Chem. Soc., 117 (1995) 9529-9534.
[20] M.I. Bethencourt, L.-o. Srisombat, P. Chinwangso, T.R. Lee, SAMs on Gold Derived from the Direct Adsorption of Alkanethioacetates Are Inferior to Those Derived from the Direct Adsorption of Alkanethiols, Langmuir, 25 (2009) 1265-1271.
[21] A. Singh, D.H. Dahanayaka, A. Biswas, L.A. Bumm, R.L. Halterman, Molecularly Ordered Decanethiolate Self-Assembled Mono layers on Au(111) from in Situ Cleaved Decanethioacetate: An NMR and STM Study of the Efficacy of Reagents for Thioacetate Cleavage, Langmuir, 26 (2010) 13221-13226.
[22] K.H.A. Lau, C. Huang, N. Yakovlev, Z.K. Chen, S.J. O'Shea, Direct adsorption and monolayer self-assembly of acetyl-protected dithiols, Langmuir, 22 (2006) 2968-2971.
[23] P. Piotrowski, J. Pawlowska, J. Pawlowski, A. Wieckowska, R. Bilewicz, A. Kaim, Nanostructured films of in situ deprotected thioacetyl-functionalized C-60-fullerenes on a gold surface, J. Mater. Chem. A, 2 (2014) 2353-2362.
[24] H. Valkenier, E.H. Huisman, P.A. van Hal, D.M. de Leeuw, R.C. Chiechi, J.C. Hummelen, Formation of High-Quality Self-Assembled Monolayers of Conjugated Dithiols on Gold: Base Matters, J. Am. Chem. Soc., 133 (2011) 4930-4939.

[25] A. Hamelin, T. Vitanov, E. Sevastyanov, A. Popov, The Electrochemical Double-Layer on sp Metal Single-Crystals - The Current Status of Data, J. Electroanal. Chem., 145 (1983) 225-264.
[26] R. Madueno, J.M. Sevilla, T. Pineda, A.J. Roman, M. Blazquez, A voltammetric study of 6-mercaptopurine monolayers on polycrystalline gold electrodes, J. Electroanal. Chem., 506 (2001) 92-98.
[27] F.P. Cometto, V.A. Macagno, P. Paredes-Olivera, E.M. Patrito, H. Ascolani, G. Zampieri, Decomposition of Methylthiolate Mono layers on Au(111) Prepared from Dimethyl Disulfide in Solution Phase, J. Phys. Chem. C, 114 (2010) 10183-10194.
[28] J.A. Fischer, V.C. Zoldan, G. Benitez, A.A. Rubert, E.A. Ramirez, P. Carro, R.C. Salvarezza, A.A. Pasa, M.E. Vela, Sulfidization of Au(111) from Thioacetic Acid: An Experimental and Theoretical Study, Langmuir, 28 (2012) 15278-15285.
[29] C. Vericat, G. Andreasen, M.E. Vela, R.C. Salvarezza, Dynamics of potential-dependent transformations in sulfur adlayers on Au(111) electrodes, J. Phys. Chem. B, 104 (2000) 302-307.
[30] C. Vericat, M.E. Vela, G. Andreasen, R.C. Salvarezza, L. Vazquez, J.A. Martin-Gago, Sulfur-substrate interactions in spontaneously formed sulfur adlayers on Au(111), Langmuir, 17 (2001) 4919-4924.
[31] C.J. Zhong, R.C. Brush, J. Anderegg, M.D. Porter, Organosulfur monolayers at gold surfaces: Reexamination of the case for sulfide adsorption and implications to the formation of monolayers from thiols and disulfides, Langmuir, 15 (1999) 518-525.
[32] D.G. Castner, K. Hinds, D.W. Grainger, X-ray photoelectron spectroscopy sulfur 2p study of organic thiol and disulfide binding interactions with gold surfaces, Langmuir, 12 (1996) 5083-5086.
[33] B.J. Lindberg, K. Hamrin, G. Johansson, U. Gelius, A. Fahlman, C. Nordling, K. Siegbahn, Molecular Spectroscopy by Means of ESCA II. Sulfur compounds. Correlation of electron binding energy with structure, Physica Scripta, 1 (1970) 286.
[34] A.S. Duwez, Exploiting electron spectroscopies to probe the structure and organization of self-assembled monolayers: a review, J. Electron. Spectrosc. Relat. Phenom., 134 (2004) 97-138.

[35] J.C. Azcarate, M.A. Floridia Addato, A. Rubert, G. Corthey, G.S. Kuerten Moreno, G. Benitez, E. Zelaya, R.C. Salvarezza, M.H. Fonticelli, Surface Chemistry of Thiomalic Acid Adsorption on Planar Gold and Gold Nanoparticles, Langmuir, 30 (2014) 1820-1826.
[36] Y.W. Yang, L.J. Fan, High-resolution XPS study of decanethiol on Au(111): Single sulfur-gold bonding interaction, Langmuir, 18 (2002) 1157-1164.
[37] A. Shaporenko, M. Elbing, A. Baszczyk, C. von Hanisch, M. Mayor, M. Zharnikov, Self-assembled monolayers from biphenyldithiol derivatives: Optimization of the deprotection procedure and effect of the molecular conformation, J. Phys. Chem. B, 110 (2006) 4307-4317.
[38] G.T. Qin, R. Zhang, B. Makarenko, A. Kumar, W. Rabalais, J.M.L. Romero, R. Rico, C.Z. Cai, Highly stable, protein resistant thin films on SiC-modified silicon substrates, Chem. Commun., 46 (2010) 3289-3291.
[39] F. Meiners, J.H. Ross, I. Brand, A. Buling, M. Neumann, P.J. Koster, J. Christoffers, G. Wittstock, Modification of silicon oxide surfaces by monolayers of an oligoethylene glycol-terminated perfluoroalkyl silane, Colloid Surface A, 449 (2014) 31-41.
[40] M. Cerruti, S. Fissolo, C. Carraro, C. Ricciardi, A. Majumdar, R. Maboudian, Poly(ethylene glycol) monolayer formation and stability on gold and silicon nitride substrates, Langmuir, 24 (2008) 10646-10653.
[41] C.M. Lilley, Q.J. Huang, Surface contamination effects on resistance of gold nanowires, Appl. Phys. Lett., 89 (2006).
[42] J.M. Lázaro Martínez, E. Rodríguez-Castellón, R.M.T. Sánchez, L.R. Denaday, G.Y. Buldain, V. Campo Dall' Orto, XPS studies on the Cu(I,II)–polyampholyte heterogeneous catalyst: An insight into its structure and mechanism, J. Mol. Catal. A-Chem., 339 (2011) 43-51.
[43] A.J. Bard, L.R. Faulkner, Electrochemical Methods: Principles and Applications, 2ª ed., John Wiley and Sons, New York, 2001.
[44] J. Kuta, E. Yeager, Influence of Cations on Electrode-Kinetics of Ferricyanide Ferrocyanide System on Rotating Gold Electrode, J. Electroanal. Chem., 59 (1975) 110-112.
[45] R. Madueno, D. Garcia-Raya, A.J. Viudez, J.M. Sevilla, T. Pineda, M. Blazquez, Influence of the solution pH in the 6-mercaptopurine self-assembled monolayer (6MP-SAM) on a Au(111) single-crystal electrode, Langmuir, 23 (2007) 11027-11033.

[46] M. Baghbanzadeh, C.M. Bowers, D. Rappoport, T. Żaba, L. Yuan, K. Kang, K.-C. Liao, M. Gonidec, P. Rothemund, P. Cyganik, A. Aspuru-Guzik, G.M. Whitesides, Anomalously Rapid Tunneling: Charge Transport across Self-Assembled Monolayers of Oligo(ethylene glycol), J. Am. Chem. Soc., 139 (2017) 7624-7631.
[47] D.J. Vanderah, R.S. Gates, V. Silin, D.N. Zeiger, J.T. Woodward, C.W. Meuse, G. Valincius, B. Nickel, Isostructural self-assembled monolayers. 1. Octadecyl 1-thiaoligo(ethylene oxides), Langmuir, 19 (2003) 2612-2620.
[48] R. Madueno, T. Pineda, J.M. Sevilla, M. Blazquez, An electrochemical study of the SAMs of 6-mercaptopurine (6MP) at Hg and Au(111) electrodes in alkaline media, Langmuir, 18 (2002) 3903-3909.
[49] X. Xuan, Y. Wang, N. Wang, Density functional theory calculations of structure, FT-IR and Raman spectra of S-phenyl thioacetate, Spectrochim. Acta, Part A, 81 (2011) 236-241.
[50] J.K. Newman, Infrared Absorption Frequencies of Complex Thiol Esters, Spectrochim. Acta, Part A, A 25 (1969) 897-&.
[51] L. Mary Novena, S. Suresh Kumar, S. Athimoolam, K. Saminathan, B. Sridhar, Single crystal, vibrational and computational studies of Theophylline (a bronchodilator drug) and its chloride salt, J. Mol. Struct., 1133 (2017) 294-306.
[52] M. Kobayashi, M. Sakashita, Morphology Dependent Anomalous Frequency-Shifts of Infrared-Absorption Bands of Polymer Crystals - Interpretation in Terms of Transition Fipole -Dipole Coupling Theory, J. Chem. Phys., 96 (1992) 748-760.
[53] P. Harder, M. Grunze, R. Dahint, G.M. Whitesides, P.E. Laibinis, Molecular conformation in oligo(ethylene glycol)-terminated self-assembled monolayers on gold and silver surfaces determines their ability to resist protein adsorption, J. Phys. Chem. B, 102 (1998) 426-436.
[54] D.J. Vanderah, J. Arsenault, H. La, R.S. Gates, V. Silin, C.W. Meuse, G. Valincius, Structural variations and ordering conditions for the self-assembled monolayers of HS(CH2CH2O)(3-6)CH3, Langmuir, 19 (2003) 3752-3756.
[55] S. Tokumitsu, A. Liebich, S. Herrwerth, W. Eck, M. Himmelhaus, M. Grunze, Grafting of alkanethiol-terminated poly(ethylene glycol) on gold, Langmuir, 18 (2002) 8862-8870.
[56] M. Legraverend, D.S. Grierson, The purines: Potent and versatile small molecule inhibitors and modulators of key biological targets, Bioorg. Med. Chem., 14 (2006) 3987-4006.

[57] A. Stefanachi, O. Nicolotti, F. Leonetti, S. Cellamare, F. Campagna, M.I. Loza, J.M. Brea, F. Mazza, E. Gavuzzo, A. Carotti, 1,3-Dialkyl-8-(hetero)aryl-9-OH-9-deazaxanthines as potent A2B adenosine receptor antagonists: Design, synthesis, structure–affinity and structure–selectivity relationships, Bioorg. Med. Chem., 16 (2008) 9780-9789.

[58] A. Kolate, D. Baradia, S. Patil, I. Vhora, G. Kore, A. Misra, PEG — A versatile conjugating ligand for drugs and drug delivery systems, J. Controlled Release, 192 (2014) 67-81.

[59] J.S. Suk, Q. Xu, N. Kim, J. Hanes, L.M. Ensign, PEGylation as a strategy for improving nanoparticle-based drug and gene delivery, Adv. Drug Deliver. Rev., 99 (2016) 28-51.

[60] P.L. Turecek, M.J. Bossard, F. Schoetens, I.A. Ivens, PEGylation of Biopharmaceuticals: A Review of Chemistry and Nonclinical Safety Information of Approved Drugs, J. Pharm. Sci., 105 (2016) 460-475.

Graphical Abstract.